A Continuous Wave and Pulsed EPR Characterization of the Mn^{2+} Binding Site in *Rhodobacter sphaeroides* Cytochrome *c* Oxidase†

Matthew P. Espe,‡,§ Jonathan P. Hosler,‖,⊥ Shelagh Ferguson-Miller,‖ Gerald T. Babcock,‡ and John McCracken*,‡

Departments of Chemistry and Biochemistry, Michigan State University, East Lansing, Michigan 48824

Received October 24, 1994; Revised Manuscript Received March 7, 1995⊗

ABSTRACT: The ligation environment of the tightly bound Mn^{2+} in cytochrome *c* oxidase from *Rhodobacter sphaeroides* has been characterized by electron paramagnetic resonance (EPR) and electron spin echo envelope modulation (ESEEM). The EPR data show that the Mn^{2+} is six-coordinate and located in a highly symmetric binding site. Analyses of X- and Q-band EPR spectra show that the zero field splitting parameter D is 115 ± 25 G (0.0107 ± 0.0023 cm^{-1}) in the fully oxidized enzyme and 125 ± 15 G (0.0117 ± 0.0014 cm^{-1}) in the fully reduced enzyme. For both redox forms of the enzyme the value of E is ≤25 G (0.0023 cm^{-1}). By comparison with crystal structures of Mn^{2+} binding proteins, the structural changes at the Mn^{2+} binding site upon redox state change of the enzyme are estimated to be ≤0.2 Å in ligand bond lengths and ≤10° in bond angle. This analysis indicates that little modification occurs at the Mn^{2+} site upon redox change at the other metal centers. Considering the proximity of the Mn^{2+} site to heme *a* and heme a_3−Cu_B [Hosler, J. P., Espe, M. P., Zhen, Y., Babcock, G. T., & Ferguson-Miller, S. (1995) *Biochemistry 34,* 7586−7592], we interpret these results to imply also that there is no large protein conformational change near the heme *a* and heme a_3−Cu_B sites upon a change in their redox states. Multifrequency 3-pulse ESEEM results provide direct evidence for a nitrogen ligand to the Mn^{2+}, which is assigned to a histidine by comparison with ESEEM studies of Mn^{2+}-bound lectins [McCracken, J., Peisach, J., Bhattacharyya, L., & Brewer, F. (1991) *Biochemistry 30,* 4486−4491] and specifically to His-411 in subunit 1 on the basis of mutagenesis studies (Hosler et al., 1995). From these results a partial model of the Mn^{2+} binding site has been constructed.

Cytochrome *c* oxidase, a multisubunit integral membrane protein, is the terminal oxidase of the respiratory chain in mitochondria and in many aerobic bacteria. This enzyme catalyzes the reduction of oxygen to water and couples these electron-transfer processes to the transport of protons across the membrane to establish a membrane potential [reviewed in Babcock and Wikstrom (1992)].

The aa_3-type cytochrome *c* oxidase from bacteria sources has a simpler structure than the eukaryotic enzyme, but shows strong sequence homology and is functionally equivalent (Ludwig, 1987; Saraste, 1990), making it a useful model for structure−function analysis. The enzyme contains four redox-active metal centers: heme *a*, heme a_3, and Cu_A located in subunit I and Cu_B located in subunit II. These subunits are highly homologous to the mammalian enzyme (Hosler et al., 1993). Additional non-redox-active metal centers are present in cytochrome *c* oxidases, but their roles are not clear and their content varies in different species. Beef heart oxidase contains one zinc and one magnesium per enzyme monomer (Einarsdottir et al., 1985; Buse & Steffens, 1991). Metal analysis on aa_3-oxidase from *Paracoccus denitrificans* also reveals magnesium and, in addition, tightly bound substochiometric manganese (Buse & Steffens, 1991). Tightly bound Mn has been observed in several bacterial oxidases (Numata et al., 1989; Lauraeus et al., 1991; Hosler et al., 1992), but not in cytochrome *c* oxidase from eukaryotes (Buse & Steffens, 1991; Einarsdottir et al., 1985).

Although enzyme-bound Mn is not redox active, previous studies have shown that the Mn EPR spectrum is dependent on the oxidation state of the enzyme (Seelig et al., 1981; Haltia, 1992). Upon reduction of the enzyme, the EPR[1] spectrum changes by acquiring a more axial line shape and a narrower line width. The change in the EPR spectrum of Mn has been proposed to reflect a significant conformational change in the enzyme (Haltia, 1992).

Our studies on site-directed mutants of *Rhodobacter sphaeroides* cytochrome *c* oxidase have demonstrated that the conserved residues His-411 and Asp-412 of subunit I are likely ligands to the Mn (Hosler et al., 1995). Previously, these residues have been shown to be close to both the heme a_3−Cu_B center and heme *a* (Hosler et al., 1994). Evidence has also been provided which suggests that Mn is binding to the site which is otherwise occupied by Mg in cytochrome *c* oxidase (Hosler et al., 1995). While the relevance of the

† This work was supported by National Institutes of Health Grants GM45795 (J.M.), GM 25480 and GM 37300 (G.T.B.), and GM26916 (S.F.-M.); The Research Excellence Fund, State of Michigan; and The All University Research Initiation Grant, Michigan State University (J.P.H. and S.F.-M.).

‡ Department of Chemistry.

§ Present address: Department of Chemistry, Campus Box 1134, Washington University, St. Louis, MO 63130.

‖ Department of Biochemistry.

⊥ Present address: Department of Biochemistry, The University of Mississippi Medical Center, 2500 N. State Street, Jackson, MS 39216.

⊗ Abstract published in *Advance ACS Abstracts,* June 1, 1995.

[1] Abbreviations: EPR, electron paramagnetic resonance; ESEEM, electron spin echo envelope modulation; FWHM, full width at half-maximum; zfs, zero field splitting; CW, continuous wave; EXAFS, extended X-ray absorption fine structure; ENDOR, electron nuclear double resonance.

0006-2960/95/0434-7593$09.00/0

Mn binding site and its location with respect to the other metals in subunit I is now more clear, the structure of the binding site itself remains to be fully defined.

This paper details an EPR and ESEEM study of the Mn binding site in *Rb. sphaeroides* cytochrome *c* oxidase, taking advantage of our ability to prepare the enzyme with levels of Mn ranging from zero to near stochiometric. In particular, the ligation environment of the Mn has been examined in the oxidized and reduced enzyme to determine the extent of the structural perturbation that occurs at the Mn binding site with changes in the redox state of the enzyme. By using ESEEM we have also observed a nitrogen ligand to the Mn, consistent with mutational analysis (Hosler et al., 1995). These results were used to construct a partial model of the Mn binding site.

MATERIALS AND METHODS

Cytochrome *c* oxidase was purified from *Rb. sphaeroides* by a procedure described previously (Hosler et al., 1992). Adventitious Mn was removed by washing the enzyme with EDTA (Hosler et al., 1995). For EPR studies the enzyme was in a buffer containing 1% lauryl maltoside, 50 mM KH_2PO_4, and 2.5 mM KCl at pH = 7.2. The stoichiometry of bound Mn is controlled by the manganese concentration in the growth medium for the cells (Hosler et al., 1995). The enzyme concentration of purified cytochrome *c* oxidase was determined from the absolute absorbance at 605 nm by using an extinction coefficient of 40 mM^{-1} cm^{-1}. Reduced enzyme was generated by adding freshly prepared aqueous $Na_2S_2O_4$ to a final concentration of 10 mM and incubating the sample for 10 min at 4 °C. For EPR experiments approximately 200 μL of sample (30−100 μM) was loaded into a 4-mm O.D. quartz EPR tube and frozen and stored at 77 K. A sample size of approximately 75 μL was used for the pulsed EPR experiments. The beef heart oxidase sample is 200 μM.

In the EPR spectra of the oxidized enzyme (Figure 1A,C), the signals arising from heme *a* and Cu_A were removed by subtracting the EPR spectrum (acquired at 10 and 110 K) of oxidase isolated from *Rb. sphaeroides*, grown in the presence of 0.5 μM Mn. Under these growth conditions there is no EPR-detectable Mn bound to the oxidase [Figure 1 in Hosler et al. (1995)].

EPR. X-band EPR spectra were recorded on a Bruker ER200 series spectrometer by using a TE_{102} cavity. Sample temperature of 110 K was achieved with flowing N_2 gas that was cooled with liquid nitrogen. The EPR cryostat was home-built and based on the Bruker design. Rapid N_2 flow rates were used to minimize thermal gradients in the sample. For data collected at 10 K an Oxford ESR-9 liquid He flow cryostat was used. The *g*-values were determined by direct measurement of the magnetic field and microwave frequency by using a Bruker ER035M NMR gaussmeter and an EIP25B frequency counter. Q-band EPR spectra were recorded on a Bruker ESP300 spectrometer (Dr. R. Hille, Dept. of Medical Biochemistry, Ohio State University) equipped with an ER035M gaussmeter and a Hewlett-Packard 5352B microwave frequency counter.

ESEEM. The pulsed EPR experiments were performed on a home-built spectrometer described elsewhere (McCracken et al., 1992). The ESEEM data were collected by using the three-pulse (90°-τ-90°-T-90°) stimulated echo sequence. The time τ between the first and second microwave pulses was set to an integer multiple of the proton Larmor precession period, to suppress the ESEEM from "matrix" protons. The time T between the second and third pulses was scanned from an initial value of τ + 40 ns to 5 μs with an interval between data points of 5 ns. All three pulses had the same width (15 ns FWHM) and power. The data were acquired at 2 K by using a liquid helium immersion system. This temperature was chosen since better echo signal/noise ratios were obtained; other than changes in signal/noise, the spectra recorded at 2 K were the same as those obtained at 4.2 K. The acquisition rate was 30 Hz, and each time point was the average of 30 events. The remainder of the experimental conditions are listed in the figure captions. The ESEEM spectra were obtained by Fourier transformation and the dead-time reconstruction technique of Mims (1984).

EPR Analysis. The EPR spectrum of Mn^{2+} has been studied in detail (Reed & Markham, 1984) and can be described by the Hamiltonian

$$\mathcal{H} = g\beta HS_Z - g_N\beta_N HI_Z + AS_ZI_Z + D[S_Z^2 - 3S(S+1)] + E(S_X^2 - S_Y^2) + IA_{SHF}S \quad (1)$$

where g and A, the ^{55}Mn hyperfine coupling constant, are assumed isotropic. D and E are the zero field splitting (zfs) tensor parameters. The last term in eq 1 describes the superhyperfine coupling between the unpaired electrons and spatially close nonzero spin nuclei. The zfs parameters D and E provide insight into the symmetry of the Mn^{2+} ligation sphere. Large D values and E/D ratios are characteristic of a less symmetric site. For Mn^{2+}, $S = 5/2$ and there are five fine structure transitions arising from transitions between the six electronic states, $M_S = \pm5/2, \pm3/2, \pm1/2$. Each of the five fine structure transitions is split into six lines from hyperfine coupling to the ^{55}Mn nucleus, $I = 5/2$ ($m_I = \pm5/2, \pm3/2, \pm1/2$), and there are 30 allowed transitions. The energies of the $M_S = \pm5/2$ and $\pm3/2$ states are dependent to first order on D and E, and thus on the angle of the applied magnetic field relative to the molecular axis system (Reed & Markham, 1984). In frozen solution samples, as studied here, all molecular orientations are present. The angular dependence of the $M_S = \pm5/2$ and $\pm3/2$ states results in line shapes that can cover several thousand Gauss; the intensities of these EPR transitions are weak and commonly difficult to observe in CW-EPR experiments of powder samples. The energies of the $M_S + \pm1/2$ states are not dependent on D and E to first order and show only a small angular dependence. The $M_S = -1/2 \rightarrow +1/2$ transition is therefore much more intense than the other fine structure transitions and is the dominant signal in a powder sample. For Mn^{2+} in cytochrome *c* oxidase, this is the only fine structure transition observed in the EPR spectrum.

In addition to the allowed transitions, there are forbidden transitions of the type $|M_S, m_I\rangle \rightarrow |M_S - 1, m_I \pm 1\rangle$. There are two forbidden transitions between each allowed transition. The amplitudes of the forbidden transitions, relative to the allowed transitions, increase with increasing D and E and decrease at higher microwave frequency where the electronic Zeeman term dominates the spin Hamiltonian. Increasing the microwave frequency from X-band (9 GHz) to Q-band (35 GHz) then simplifies the EPR spectrum.

EPR Simulations. The Q-band simulation routine used was developed by Dr. G. Reed (Markham et al., 1979). The

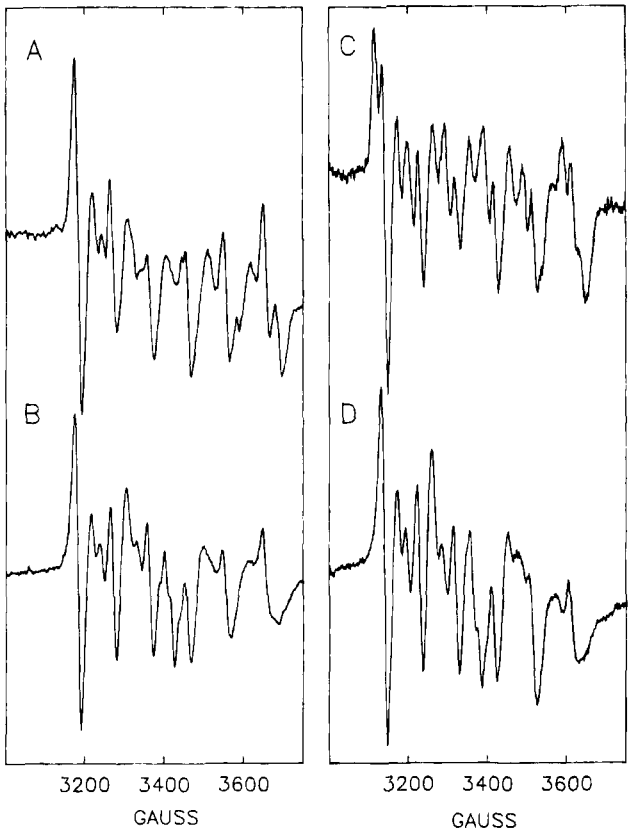

FIGURE 1: EPR spectra of *Rb. sphaeroides* oxidase in the fully oxidized (A and C) or fully reduced (B and D) forms. For the oxidized samples the signals from cyt *a* and Cu_A have been subtracted (see Materials and Methods). Conditions (A and B): microwave power, 20 mW; microwave frequency, 9.592 GHz; modulation, 12.5 Gpp; temperature, 110 K; (C and D) microwave power, 2.0 mW; microwave frequency, 9.467 GHz; modulation, 12.5 Gpp; temperature, 10 K.

energy levels were calculated to third order by using perturbation theory. The input parameters were *g*-value, Mn hyperfine coupling, *D*, *E*, and line width. The hyperfine coupling and *g*-values are isotropic. Both allowed and forbidden transitions are calculated for the $M_S = -1/2 \rightarrow +1/2$ transition. The errors reported for the simulation results were determined from visual inspection of the simulated and experimental data.

RESULTS

X-Band EPR. The $g = 2.0$ region of the low-temperature EPR spectrum from oxidized *Rb. sphaeroides* cytochrome *c* oxidase contains signals from heme *a* and Cu_A. When Mn^{2+} is bound to the enzyme, its EPR signal is also observed in the $g = 2.0$ region [Figure 1 in Hosler et al. (1995)]. X-band EPR spectra of oxidase-bound Mn^{2+}, from both the oxidized and reduced forms at 10 and 110 K, are shown in Figure 1. For the oxidized enzyme, the EPR signals from Cu_A and heme *a* have been removed by subtracting the EPR spectrum from *Rb. sphaeroides* oxidase sample that contained no detectable Mn (see Materials and Methods). Previously, the Mn^{2+} signal could only be observed with the overlapping Cu_A signal present (Seelig et al., 1981; Haltia, 1992; Hosler et al., 1992). In the reduced enzyme, heme *a* and Cu_A are diamagnetic and yield no EPR signal, and only the signal from Mn^{2+} is observed. In all cases, only the central fine structure transition from Mn^{2+} is detected. The differences in the EPR spectra at the two temperatures are likely to be the result of changes in the zfs parameters. Temperature dependencies in *D* and *E* have been observed for inorganic complexes of Mn^{2+} (Drumheller & Rubins, 1986; Marcos et al., 1990).

By using the splitting observed in the highest field peak and the intensity ratio of forbidden and allowed transitions in the X-band EPR spectrum at 110 K [Shaffer et al., 1976; see Weltner (1983)], we calculate *D* to be approximately 150 G (0.014 cm^{-1}) for Mn^{2+} in the oxidized enzyme. In contrast to *D*, there are no simple approaches for determining the value of *E*. However, insight into the ratio of *E* to *D* can be obtained from the line shape of the EPR spectrum (Reed & Markham, 1984). The Mn^{2+} EPR spectrum from *Rb. sphaeroides* oxidase shows a line shape similar to that observed for a creatine kinase complex with bound Mn^{2+} (Reed & Leyh, 1980). With similar line shapes the two proteins should show a similar value of *E/D* for Mn^{2+}. The values of *D* and *E* are slightly larger for creatine kinase, but the value of 0.2 for *E/D* is a good approximation for oxidase-bound Mn^{2+}. The value of *E* for oxidase-bound Mn^{2+} in the oxidized form is $\approx$30 G (0.0028 cm^{-1}). The Mn^{2+} EPR spectrum of the reduced enzyme shows slightly larger forbidden transitions than the oxidized enzyme, indicative of a small increase in the value of *D* upon reduction. In addition, the highest field peak has collapsed compared to that observed for the oxidized enzyme, consistent with a decrease in *E/D* and a likely decrease in *E* (Reed & Markham, 1984). The X-band data from oxidase, with only minor differences between the oxidized and reduced forms, show that there is little structural change at the Mn binding site with oxidation state changes of the redox-active metals.

Q-Band EPR. The *g*-values and ^{55}Mn hyperfine coupling can be more easily determined at Q-band because of the decreased intensity of the forbidden transitions. In addition, with data from a second microwave frequency and the ability to simulate the Q-band data, the zfs parameters *D* and *E* can be more accurately defined. The Q-band EPR data collected at 150 K are shown in Figure 2A,B for the oxidized and reduced enzyme, respectively. The *g*-values are the same for both redox forms of the enzyme (Table 1) and are consistent with previously reported values of protein-bound Mn^{2+} (Reed & Markham, 1984). The value of the Mn hyperfine coupling (Table 1) is indicative of a six-coordinate ligation environment consisting of "hard" ligands such as oxygen and nitrogen (Misra & Sun, 1991). The Mn hyperfine coupling does, however, change upon reducing the enzyme. The decreased hyperfine coupling in the reduced enzyme is indicative of less unpaired spin density on the metal and more on the ligands; this can be accomplished by increasing the covalency of one or more of the ligands in the reduced enzyme.

The values of *D* and *E* for the oxidized enzyme, determined by simulation of the Q-band EPR results, are consistent with the X-band data, yielding $D = 115 \pm 25$ G (0.0107 ± 0.0023 cm^{-1}) and $E = 25 \pm 15$ G (0.0023 ± 0.0014 cm^{-1}), with $E/D = 0.22$ (Table 1; Figure 2C). For the reduced form, the simulation reveals $D = 125 \pm 20$ G (0.0117 ± 0.0014 cm^{-1}) and $E = 45 \pm 5$ G (0.0042 ± 0.00047 cm^{-1}) (Table 1; Figure 2D). The small increase in *D* observed upon reducing the enzyme is consistent with the X-band results. There is a discrepancy in the value of *E*,

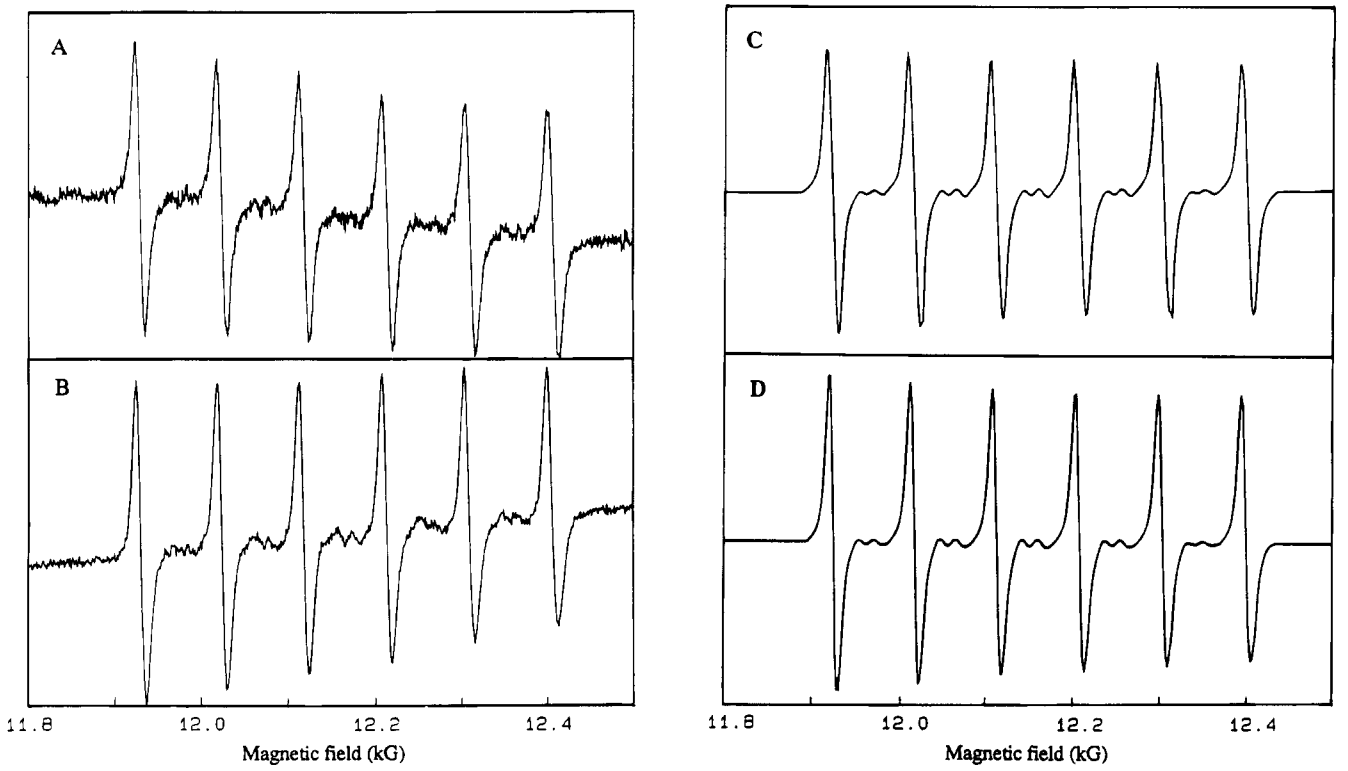

FIGURE 2: Q-band EPR spectra of (A) fully oxidized and (B) fully reduced *Rb. sphaeroides* oxidase and simulations of Q-band EPR spectra from (C) oxidized and (D) reduced enzyme. The simulation parameters are listed in Table 1. Conditions: microwave power, 1 mW; microwave frequency, 34.115 GHz; modulation, 5 Gpp; temperature, 150 K.

Table 1: EPR Parameters for Mn^{2+} Determined from Simulations of the Q-band EPR Data

oxidation state of enzyme	*g*-value	Mn hyperfine coupling (G)	*D*	*E*	line width (G)
oxidized	2.0026 ± 0.00005	95.2 ± 0.2	115 ± 25 G (0.0107 ± 0.0023 cm^{-1})	25 ± 10 G (0.0023 ± 0.00093 cm^{-1})	6.0
reduced	2.0027 ± 0.00005	94.7 ± 0.2	125 ± 15 G (0.0117 ± 0.0014 cm^{-1})	45 ± 5 G (0.0042 + 0.00047 cm^{-1})	5.0

however, between the X- and Q-band data. The simulations of the Q-band data shown an increase in *E* upon reduction, whereas the X-band data suggest that *E* decreases. Since the line shapes of the X-band data are more sensitive to the values of *D* and *E* (Reed & Markham, 1984), we favor the interpretation that *E* decreases upon enzyme reduction. The increase in the asymmetry of the high-field peaks of the Q-band data (Figure 2B) upon reduction of the enzyme, may be a result of an increase in the anisotropy of *g* and/or *A*, rather than an increase in *E*. As the line-shape changes in the X-band spectra are indicative of a decrease in *E*/*D*, and both the X- and Q-band data show that *D* increases only slightly upon enzyme reduction, *E* must be ≤25 G (0.0023 cm^{-1}) in the reduced enzyme. As described previously, the Mn^{2+} EPR signal becomes more axial in the reduced enzyme (Seelig et al., 1981; Haltia, 1992). Our results show, however, that the changes are minor (ΔD = 10 G, and ΔE ≤ 25 G).

Similar to the zfs parameters, the line widths in *Rb. sphaeroides* oxidase are also dependent on oxidation state. Table 1 shows that in the Q-band data the line width is narrower in the reduced form of the enzyme. This is also observed in the X-band data where the line width of the lowest field peak decreases from 19 to 17 G upon enzyme reduction. The change in the EPR line width is not a function of saturation properties of the EPR signal, as spectra recorded at microwave powers well below saturation show the same trend in line widths.

ESEEM. For Mn^{2+}, in most cases, superhyperfine couplings to ligand nuclei are too small to be resolved from the broad EPR line widths. ESEEM is a high-resolution technique that allows one to measure weak ligand hyperfine couplings to nuclei with non-zero spin (Mims & Peisach, 1981). Magnetic nuclei that are in the vicinity of the Mn^{2+} (<6 Å) give rise to a peak in the ESEEM spectrum at their respective Larmor frequencies. For nuclei that are ligated to the metal, the hyperfine coupling may be larger and the peaks may be split away from the Larmor frequency. Previous applications of ESEEM to study Mn binding proteins have been productive in detecting protons, nitrogens, and phosphorus that are part of, or close to, the binding site of the metal (Tipton et al., 1989; Eads et al., 1988; Tipton et al., 1991; LoBrutto et al., 1986; Halkides et al., 1994). In the ESEEM spectra of Mn^{2+} in *Rb. sphaeroides* oxidase the nuclei most likely to be observed are nitrogens and protons.

Since the ESEEM spectrum is a composite from all paramagnetic species that have EPR intensity at the magnetic field position where the experiment is performed, the ESEEM data from oxidized *Rb. sphaeroides* cytochrome *c* oxidase collected at $g = 2.01$ may show contributions from heme *a*, Cu_A, and Mn^{2+} (Hosler et al., 1992). To identify the peaks originating from Mn^{2+}, *Rb. sphaeroides* oxidase samples

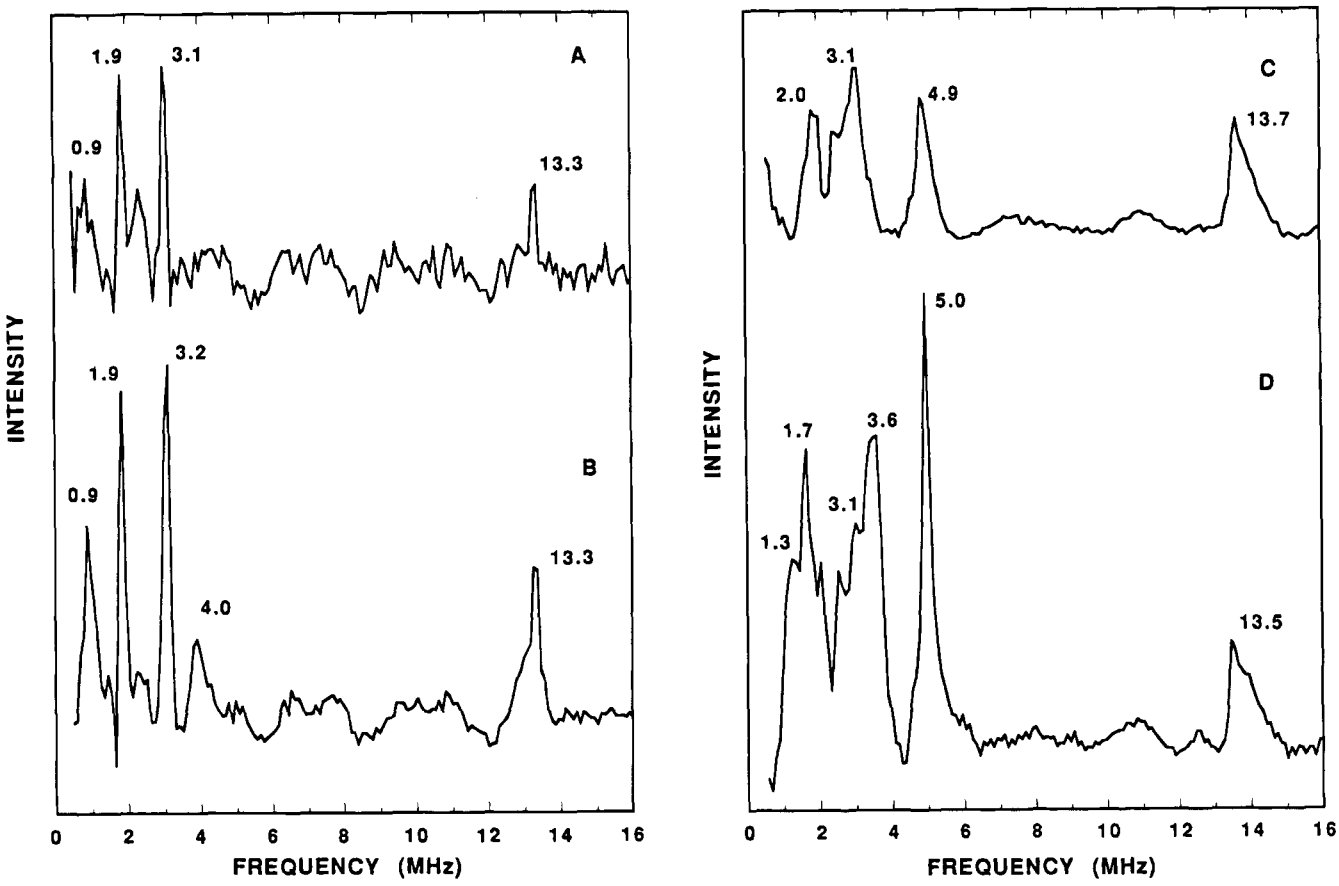

FIGURE 3: Three-pulse ESEEM spectra of (A) oxidized *Rb. sphaeroides* oxidase that contains no bound Mn, (B) beef heart oxidase, (C) oxidized *Rb. sphaeroides* oxidase containing 0.7 Mn/enzyme, and (D) reduced *Rb. sphaeroides* oxidase containing 0.7 Mn/enzyme. All spectra were collected at $g = 2.01$. Conditions: (A) microwave frequency, 8.885 GHz; magnetic field, 3160 G; (B) microwave frequency, 8.890 GHz; magnetic field, 3165 G; (C) microwave frequency, 8.980 GHz; magnetic field, 3190 G; (D) microwave frequency, 8.880 GHz; magnetic field, 3157 G; τ, 225 ns; T, 2 K. Spectra A, B, and D are single scans, and spectrum C is the average of two scans.

containing no detectable Mn and 0.7 Mn/enzyme were studied. For comparison, the beef heart enzyme was also studied. Typical three-pulse ESEEM spectra collected at 9 GHz and identical τ values of 225 ns for Mn-deficient bacterial oxidase and beef heart oxidase are shown in Figure 3. For the Mn-depleted bacterial oxidase (Figure 3A), the spectrum taken at $g = 2.01$ shows low-frequency peaks at 0.93, 1.91, 2.38, and 3.10 MHz along with a peak centered at the proton Larmor frequency, 13.33 MHz. A similar spectrum is found for the beef heart oxidase (Figure 3B), with peaks at 0.93, 1.91, 3.15, and 3.92 MHz and at the proton Larmor frequency, 13.32 MHz. These peaks are assigned to Cu_A (see below). The ESEEM spectra for the oxidized and reduced bacterial oxidase samples with 0.7 Mn/enzyme are shown in panels C and D, respectively, of Figure 3. The ESEEM spectra consist of three low-frequency peaks with complex line shapes positioned at 1.97, 3.12, and 4.92 MHz for the oxidized enzyme and 1.70, 3.57, and 5.02 for the reduced enzyme. In reduced *Rb. sphaeroides* oxidase the only paramagnet is Mn^{2+}, and thus the spectrum from this sample (Figure 3D) arises solely from enzyme-bound Mn^{2+}. The ESEEM spectrum from the oxidized bacterial enzyme containing 0.7 Mn/enzyme is a composite of the spectra from Mn^{2+} and Cu_A.

To separate the spectra from Cu_A and Mn^{2+}, ESEEM data were collected at a second magnetic field position. At $g = 1.90$, the EPR spectrum from *Rb. sphaeroides* oxidase containing Mn^{2+} shows substantial intensity from Mn^{2+}, but little contribution from Cu_A[$H = 3350$, Figure 1C in Hosler et al. (1995)]. The ESEEM spectrum of the oxidized Mn-containing bacterial oxidase collected at $g = 1.90$ (Figure 4A) shows changes in the line shape of the low-frequency peaks with increase in magnetic field strength, and slight shifts in their frequency maxima to 1.70, 2.94, and 5.02 MHz. The shift of the high-frequency peak to 14.48 MHz is consistent with the assignment of this peak to the matrix protons. Electron spin echoes were not detected at $g = 1.90$ for the oxidized bacterial oxidase that did not contain bound Mn^{2+} (data not shown). The spectrum in Figure 4A, then, arises only from oxidase-bound Mn^{2+}. The spectrum from the reduced enzyme at $g = 1.90$ is shown in Figure 4B. Comparison of the data in Figure 4 shows that the enzyme affects only minor changes in the line shapes and frequencies of the low frequency modulation components upon change in the redox state of the oxidase.

To determine whether, the low-frequency peaks in the spectra of Figure 4 arise from hyperfine coupling to nitrogen, multifrequency experiments were carried out. Figure 5 shows the ESEEM spectra for the reduced Mn-containing bacterial enzyme acquired at microwave frequencies of 8.90 and 11.20 GHz. At $g = 1.90$, this corresponds to magnetic field values of 3350 and 4200 G, respectively. Peaks arising from protons are expected to shift by 3.6 MHz between the two spectra of Figure 5, while for nitrogen the shift would be 0.6 MHz or less. Figure 5 shows that the shifts are those expected for hyperfine coupling to nitrogen. This is most

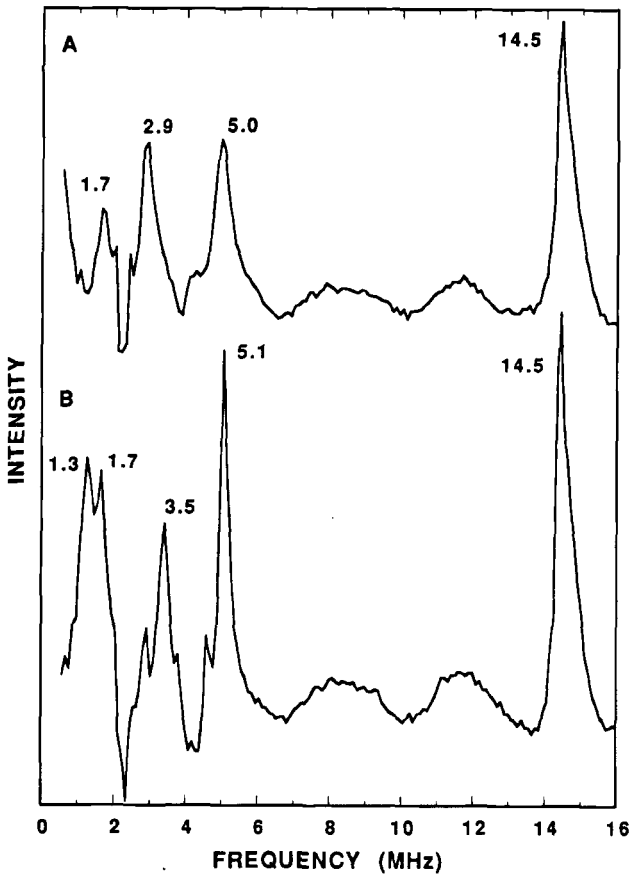

FIGURE 4: Three-pulse ESEEM spectra of (A) oxidized and (B) reduced *Rb. sphaeroides* oxidase containing 0.7 Mn/enzyme. The data were collected at $g = 1.90$. Conditions: (A) microwave frequency, 8.980 GHz; magnetic field, 3375 G; (B) microwave frequency, 8.970 GHz; magnetic field, 3375 G; other conditions were as described in Figure 3. The spectra are the average of four scans.

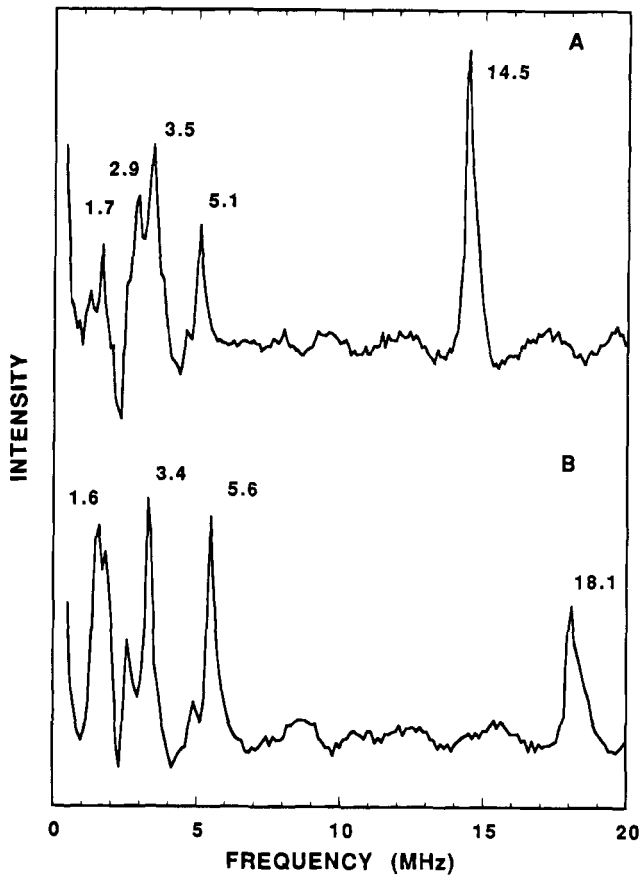

FIGURE 5: Three-pulse ESEEM spectra of reduced *Rb. Sphaeroides* oxidase at two microwave frequencies: (A) microwave frequency, 8.970 GHz; magnetic field, 3375 G; (B) microwave frequency, 11.2 GHz; magnetic field, 4226 G. Both spectra were collected at $g = 1.90$. Conditions: τ, 300 ns (A) or 232 ns (B); other conditions were as in Figure 3. Spectrum A is the average of two scans.

clearly seen for the peak at 5.1 MHz (Figure 5A) that shifts to 5.55 MHz (Figure 5B).

Since electron spin echoes were not observed at $g = 1.90$ for the oxidized *Rb. sphaeroides* oxidase lacking bound Mn^{2+} (data not shown), the peaks in the ESEEM spectrum collected at $g = 2.01$ (Figure 3A) must come from Cu_A. If there were detectable peaks in the ESEEM spectrum from heme *a*, they should still be observable at $g = 1.90$ (Peisach et al., 1979). Apparently the enzyme concentrations are too low for contributions from heme *a* to be detected. The Cu_A ESEEM spectrum from beef heart oxidase (Figure 3B) is very similar to that observed for the bacterial oxidase (Figure 3A) and to previously published data (Mims et al., 1980; Hansen et al., 1993). While the ESEEM data from Cu_A have not been fully characterized, the low-frequency peaks likely arise from nitrogen hyperfine coupling. ENDOR measurements (Stevens et al., 1982) have shown that Cu_A contains at least one histidine ligand, and EXAFS results suggest that there may be two histidine ligands (Li et al., 1987). Two histidine ligands to Cu_A are also predicted from mutagenesis studies of the membrane-exposed region of subunit II (Kelly et al., 1993). An EPR characterization of the *Rb. sphaeroides* oxidase has already shown that the EPR signal from Cu_A is nearly identical to that observed for beef heart oxidase [Figure 1 in Hosler et al. (1995)]. The ESEEM results presented here, where hyperfine coupling to one or two of the ligands to Cu_A can be observed, provide a more detailed investigation of the Cu_A site. The similarity of the ESEEM data collected at $g = 2.01$ from beef heart and *Rb. sphaeroides* cytochrome *c* oxidase shows that this aspect of Cu_A ligation is shared between the bacterial and eukaryotic oxidases.

DISCUSSION

Characterization of the Mn Ligation Environment in Rb. sphaeroides Cytochrome c Oxidase. The zfs parameter *D* has been observed to be as large as several thousand gauss in Mn complexes (Misra & Sun, 1991) and up to 1300 G in Mn binding proteins (Reed & Markham, 1984). The value of *D* for Mn bound to *Rb. sphaeroides* cytochrome *c* oxidase, ≈120 G for both the oxidized and the reduced enzyme, is one of the lowest reported for biological systems and shows that the metal is located in a highly symmetric octahedral site. In addition, the EPR spectra, especially the Q-band data, give no indication that there is more than one type of Mn binding site present. This is consistent with the mutagenesis results that show a complete loss of Mn binding with single-site mutations of His-411 or Asp-412 (Hosler et al., 1995).

The EPR line widths of protein-bound Mn are broad, in many cases, due to a distribution in the magnitudes of *D* and *E*, which is caused by microheterogeneity in the structures of the Mn binding sites (Reed & Markham, 1984). This effect is present in *Rb. sphaeroides* oxidase as evidenced by the relatively large line widths. The line widths observed

in the X-band spectrum, 17−19 G, are significantly larger than the line widths (<5 G) observed for powder samples of some Mn^{2+} inorganic complexes (Beltran-Lopez & Castro-Tello, 1980; Kudynska et al., 1992). The EPR data show that the Mn binding site in *Rb. sphaeroides* cytochrome *c* oxidase is less heterogeneous when the enzyme is fully reduced. This result correlates well with previous EPR and optical studies of mammalian cytochrome *c* oxidase. Isolated beef heart enzyme, in its resting form, exhibits a Soret optical absorption maximum with strong contributions from both heme *a* and heme a_3 that vary over the range from 417 to 425 nm and between preparations, even when using the same purification procedure (Baker et al., 1987). EPR studies have revealed that there are three forms of the oxidized enzyme that are interconvertible and that the structural heterogeneity of the enzyme is associated with the binuclear center conformation (Brudvig et al., 1981). When studied optically, this heterogeneity is absent in the fully reduced enzyme (Babcock, 1988).

Quantitative interpretation of the three-pulse ESEEM data is not currently possible owing to the complexity of the hyperfine coupling to an $S = 5/2$ paramagnet. In the EPR spectrum of Mn^{2+} in *Rb. sphaeroides* oxidase, only the $M_s = -1/2 \rightarrow +1/2$ fine structure transition is detected, while the other four fine structure transitions are not observed owing to their weak intensity. It has recently been shown in other systems that in two-pulse ESEEM experiments the ESEEM spectra arising from the four weak EPR fine structure transitions can be detected (Larsen et al., 1993; Coffino & Peisach, 1992). Simulations of the Q-band EPR spectrum from *ras* p21, a single Mn binding protein with ^{55}Mn hyperfine coupling and *D* values similar to those of the Mn in *Rb. sphaeroides* oxidase (Smithers et al., 1990), have revealed that the five fine structure transitions severely overlap each other (Larsen et al., 1993). Simulations of the two-pulse ESEEM data from this protein have shown that the observed spectrum is a composite of the five separate ESEEM "subspectra" that arise from these overlapping fine structure transitions (Larsen et al., 1993). As spectra are recorded at different field values, the relative contributions of the fine structure transitions will change, altering the shape of the composite spectrum (Larsen et al., 1993; Coffino & Peisach, 1992). This effect is also observable in the three-pulse ESEEM spectra from Mn(II) in *Rb. sphaeroides* oxidase. The spectrum of the reduced enzyme collected at $g = 2.01$ (Figure 3D) is slightly different from the spectrum collected at $g = 1.90$ (Figure 4B). This is most clearly seen in the change in the relative amplitudes of the peaks at 1.30 and 3.06 MHz.

An understanding of the ESEEM spectra from Mn(II) in *Rb. sphaeroides* oxidase can be obtained from comparison with data from other Mn binding proteins. The ESEEM spectra from a series of lectins, including concanavalin A and pea lectin, show a set of nearly identical spectra (McCracken et al., 1991). From multifrequency studies, it was shown that the peaks originate from hyperfine coupling to one or more nitrogens. These spectra are also similar to the spectrum obtained for Mn^{2+} in the presence of an excess of imidazole (McCracken et al., 1991). As the crystal structures of concanavalin A (Becker et al., 1975; Hardman et al., 1982) and pea lectin (Einspahr et al., 1986) show a single histidine ligand to the Mn, the ESEEM spectra for these proteins were interpreted as arising from hyperfine coupling to the *ligating* histidyl nitrogen (McCracken et al., 1991). The ESEEM spectra from the reduced form of *Rb. sphaeroides* oxidase show a strong similarity to the spectra observed for pea lectin, which show peaks at 1.4, 2.0, 2.7, 3.3, and 4.9 MHz, with similar line shapes and intensities (McCracken et al., 1991). The ESEEM results from *Rb. sphaeroides* oxidase are thus indicative of a histidine ligand to the Mn. The strong similarity between the oxidase and lectin data, where it is known that there is only one nitrogen ligand, suggests that there is only one nitrogen ligand to the Mn in *Rb. sphaeroides* cytochrome *c* oxidase.

The identification of a histidine ligand to the Mn in cytochrome *c* oxidase is consistent with solved structures of Mn binding proteins where there is, in most cases, a histidine ligand (Hardman et al., 1982; Yamashita et al., 1989; Einspahr et al., 1986; Whitlow et al., 1991). His-411 is conserved in all but two of the more than 70 subunit I sequences now available [see Calhoun (1993)], implying that this amino acid performs a specific function within the enzyme. The six other completely conserved histidines in subunit I are ligands to heme *a*, heme a_3, and Cu_B (Shapleigh et al., 1992; Hosler et al., 1993). Since the subunit I mutants H411N and H411A result in loss of Mn binding (Hosler et al., 1995), His-411 is assigned as a ligand to the Mn and the source of the peaks in the ESEEM spectra.

Extent of Structural Change at the Mn Binding Site. Although the structure of the Mn binding site in the bacterial oxidase is modified upon reduction of Cu_A and heme *a* (Haltia, 1992), the small changes in the *D* and *E* values reported here indicate that the changes are minimal. From the crystal structures and previous EPR studies of Mn binding proteins, some insight into the extent of structural modification of the Mn binding site in *Rb. sphaeroides* oxidase upon reduction of the iron and copper centers can be obtained. The crystal structures of Mn binding proteins reveal some common characteristics within this class of proteins (Declercq et al., 1991; Hardman et al., 1982; Yamashita et al., 1989; Einspahr et al., 1986; Whitlow et al., 1991). In almost all cases, protein ligands to the Mn are glutamate, aspartate, or histidine. One or two water molecules are also commonly ligands to the metal, and in some cases the ligand sphere is completed with a backbone carbonyl. The ligand geometry around the metal is six-coordinate, with a near octahedral geometry, in the proteins characterized to date. In all cases, moderate distortions away from this octahedral symmetry occur. Bond angles between ligands *cis* to each other range form 63 to 121°, and the angle between *trans* ligands ranges from 151 to 177°. The bond lengths can also vary considerably. The Mn−O bond lengths for glutamates and aspartates lie in the range 1.92−2.37 Å, and the Mn−N distances for histidines cover a smaller range, 2.2−2.3 Å. For bound water, the observed bond lengths are 2.0−2.3 Å. The larger the variation in bond angles and bond lengths, the larger are the zfs parameters *D* and *E*.

For concanavalin A (Hardman et al., 1982) and parvalbumin (Declercq et al., 1991), where highly refined protein structures have been determined, the geometric parameters of the Mn binding site encompass the full range of values discussed above. For concanavalin A, the metal ligand bond lengths are very nearly equal, while the bond angles cover the ranges described above (Hardman et al., 1982). The opposite is seen for parvalbumin, where the bond angles cover a small range and are near the values expected for

octahedral symmetry, while the bond lengths differ by 0.5 Å (Declercq et al., 1991). EPR studies of these proteins reflect these distortions with larger D and E values. Detailed simulations of the X- and Q-band EPR spectra for concanavalin A show that $D = 230$ G and $E = 46$ G (Meirovich & Poupko, 1978). For paravalbumin the value of D was estimated to be 400 G, while E was not determined (Harshore & Boucher, 1974). The small changes for D and E observed upon redox change at the heme irons and coppers in *Rb. sphaeroides* oxidase ($\Delta D = 10$ G; $\Delta E \leq 25$ G) thus represent only minor changes in the structure of the Mn^{2+} binding site. From the crystal structures and EPR data of the Mn binding proteins discussed above, we estimate that the redox-mediated structural changes that occur at the Mn binding site in the bacterial cytochrome *c* oxidase are <0.2 Å in bond length and <10° in bond angle. These changes are cumulative over the six ligands.

The Mn^{2+} X-band EPR spectra presented here for the oxidized and reduced *Rb. sphaeroides* enzyme are very similar to those reported for cytochrome *c* oxidase from *P. denitrificans* (Haltia, 1992). The change in the Mn^{2+} EPR spectrum in *P. denitrificans* oxidase in going from the fully oxidized to the reduced form of the enzyme is attributed to the Mn being in "dissimilar coordination environments" (Haltia, 1992). In contrast, by using a more detailed analysis, we have determined that the structural changes at the Mn binding site in *Rb. sphaeroides* oxidase, upon full redox change of the enzyme, are small, as described above.

The positions of the peaks in the ESEEM spectrum are dependent on the hyperfine and quadrupole couplings. These values are, in turn, dependent on the Mn−N_{His} bond length, the extent of covalency in the bond, and the unpaired spin density residing on the Mn. Since the ESEEM spectrum is a composite of ESEEM "subspectra" arising from each of the fine structure transitions, changes in the zfs parameters from changes in the binding site geometry will also affect the ESEEM spectrum. The changes in the ESEEM spectra between the oxidized and reduced enzyme are minor (Figure 4), again indicating that the structural changes that occur at the Mn binding site, as suggested by the EPR data, are slight.

Mn as a Monitor of Cytochrome Oxidase Conformational States. It remains unresolved whether cytochrome *c* oxidase undergoes large conformational transitions upon electron filling or protonation events (Jensen et al., 1984; Baker et al., 1987) or the changes are small and restricted to local rearrangements near the redox-active metals (Moody et al., 1991; Mitchell et al., 1992). Since the proposed Mn ligand His-411 is close to the heme a_3−Cu_B center and the "indirect" ligand Asp-412 (see below) is located between heme *a* and heme a_3 (Hosler et al., 1984), the Mn center should be sensitive to conformational changes in both of these redox-active centers. Haltia (1992) has concluded that changes in Mn coordination geometry correspond to the reduction of heme *a* and Cu_A but not the heme a_3−Cu_B center. Our results are generally in agreement with this, since the reduction of the entire enzyme yields a Mn EPR spectrum very similar to that of the mixed-valence form examined by Haltia. Thus, no additional structural modification at or near the Mn binding site is observed in going from the two electron reduced enzyme to the fully reduced form. The changes, however, that occur in the geometry of the Mn center upon reduction and oxidation of the redox-active metals of *Rb. sphaeroides* oxidase are small, as shown by the EPR and ESEEM analyses. This suggests that any conformational changes that occur near the heme *a* or heme a_3−Cu_B sites in cytochrome *c* oxidase upon redox cycling are not extensive. The EPR and ESEEM results cannot, however, exclude the possibility that there are protein conformational changes occurring away from the vicinity of the Mn binding site.

A Partial Model of the Mn Binding Site. By using the EPR, ESEEM, and subunit I mutagenesis results, in conjunction with the crystal structures of Mn binding proteins, a partial model of the Mn binding site in *Rb. sphaeroides* oxidase can be constructed. The relatively large zfs parameters for concanavlin A and parvalbumin suggest that the Mn^{2+} sites in these proteins are poor models for the Mn^{2+} site in *Rb. sphaeroides* oxidase. The EPR data for a series of plant lectins, however, show smaller zfs parameters, $D =$ 140−170 G (Meirovich et al., 1978). The X- and Q-band EPR spectra from the plant lectins are also very similar to the spectra of the oxidase-bound Mn^{2+}. The lectin from pea has also been studied by EPR; however, the value of D was not determined (Bhattacharyya et al., 1985). Comparison of the pea lectin EPR data with the data from the other plant lectins suggests that the value of D for the pea lectin is similarily in the range of 140−170 G. The crystal structure of pea lectin shows small variations in bond angles that are close to the ideal of 90° and 180° (Einspahr et al., 1986). The bond distances are also grouped closer together and are close to the average for Mn binding proteins. This more symmetric environment of the Mn binding site in pea lectin correlates well with the estimated value of D.

With the similarity in EPR and ESEEM data between pea lectin and *Rb. sphaeroides* cytochrome *c* oxidase, the structure of the Mn binding site in this lectin was used as a template to construct a model for the Mn binding site in oxidase. Ligands to the metal in the oxidase site include a nitrogen from the imidazole group of His-411 and possibly an oxygen from Asp-412. Since aspartates have a carboxyl group, this side chain may act as a bidentate ligand. In addition, previous studies by EPR of the closely related cytochrome *c* oxidase from *P. denitrificans* have shown that there is at least one water bound to the metal (Haltia, 1992). The two residues plus the water may account for as many as four of the six ligands. Within this context, modeling was done to investigate reasonable ligation environments.

Efforts to develop a model where Asp-412 acts as a bidentate ligand with His-411 also as a ligand were not successful. No side-chain orientation allowed reasonable bond lengths or angles. If the ligand environment is relaxed so that Asp-412 is a monodentate ligand, a model with O_{Asp} and N_{His} *trans* to each other with an angle of 170° can be constructed. This bond angle is very similar to that observed in pea lectin. In this model, however, there is a limited range of orientations that the protein backbone can take to position the two side chains for metal ligation. Regardless of position, the protein backbone sterically hinders access to the metal over a large enough region to eliminate the possibility of near octahedral symmetry. This model suggests that simultaneous ligation of His-411 and Asp-412 to Mn is unlikely. This is consistent with the known crystal structures of Mn binding proteins where the nearest ligating residues sequentially in the protein are two residues apart (Declercq et al., 1991; Hardman et al., 1982; Yamashita et al., 1989; Einspahr et al., 1986; Whitlow et al., 1991).

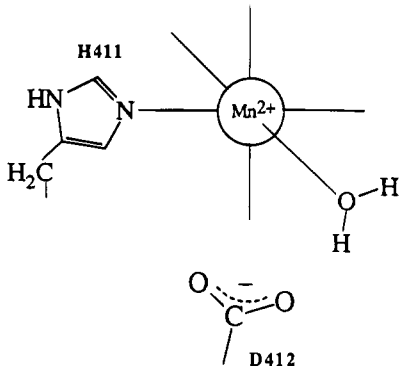

FIGURE 6: A partial model of the Mn binding site in *Rb. sphaeroides* cytochrome *c* oxidase. While Asp-412 is shown as deprotonated, the actual protonation state of this residue is not known. Details of the model are provided in the text.

While His-411 and Asp-412 are both important in constructing the Mn binding site, they may serve different roles. From the ESEEM data the histidine is assigned as a ligand, whereas Asp-412 may serve as a hydrogen bond acceptor and form a hydrogen bond with the water molecule ligated to the metal. A model with the Nε nitrogen of histidine as the ligand to Mn with a bond length of 2.20 Å, a $Mn-O_{H_2O}$ bond length of 2.15 Å, and a $N_{His}-Mn-O_{H_2O}$ angle equal to 90° yields a metal binding site with characteristics similar to those observed in pea lectin. The side chain of Asp-412 can then easily form a hydrogen bond with the water, and there are four open ligand sites for metal binding (Figure 6). The crystal structures of several Mn binding proteins show hydrogen bonds between ligand water molecules and aspartates or glutamates (Declercq et al., 1991; Hardman et al., 1982). From ESEEM studies of *ras* p21, it has been determined that an aspartate residue is indirectly coordinated to the Mn through a water molecule (Halkides et al., 1994). Such a model for the Mn^{2+} site in *Rb. sphaeroides* oxidase is also consistent with the mutagenesis results reported in the accompanying paper (Hosler et al., 1995) in that mutation of His-411 or Asp-412 causes either the loss of a ligand or the loss of an important hydrogen bond, both of which would disrupt the metal binding site and cause loss of the metal.

Relationship of Mn and Mg Binding by Cytochrome c Oxidase. The physiological role of the Mn binding site remains to be determined. While Mn and Mg appear to be competitive for the metal binding site (Hosler et al., 1995), it is unclear whether the competition occurs at the level of insertion into the enzyme or uptake into the cell. It is important to note that many Mg-specific binding sites in proteins readily exchange Mn for Mg (Reed & Markham, 1984). In parvalbumin, the metal binding sites bind Mn more tightly than Mg even though the sites are occupied by Mg under physiological conditions (Declerq et al., 1991). In addition, there is both crystallographic (Declerq et al., 1991; Whitlow et al., 1991) and spectroscopic evidence (Latwesen et al., 1992; Larsen et al., 1992) that shows that substitution of Mn for Mg results in only a slight structural modification to the metal binding site. The substitution of Mn and Mg is consistent with their preferred ligation environments since both metals favor a six-coordinate, octahedral site with oxygen and nitrogen ligands (Martin, 1990). The proposed structure for the Mn binding site in the bacterial oxidase has the structural characteristics that would predict Mg as well as Mn binding. It is likely, then, that the Mn binding site in *Rb. sphaeroides* cytochrome *c* oxidase is reporting the location of the Mg site found in cytochrome *c* oxidases.

ACKNOWLEDGMENT

We thank Dr. Russ Hille for use of his Q-band spectrometer and technical assistance. We thank Dr. George Reed for providing the source code for the Q-band EPR simulation routine.

REFERENCES

Babcock, G. T. (1988) in *Biological Applications of Raman Spectroscopy* (Spiro, G. T., Ed.) pp 294–346, John Wiley and Sons, New York.
Babcock, G. T., & Wikstrom, M. (1992) *Nature 356*, 301–309.
Baker, G. M., Noguchi, M., & Palmer, G. (1987) *J. Biol. Chem. 262*, 595–604.
Becker, J. W., Reeke, G. N., Wang, J. L., Cunningham, B. A., & Edelman, G. M. (1975) *J. Biol. Chem. 250*, 1513–1524.
Beltran-Lopez, V., & Castro-Tello, J. (1980) *J. Magn. Reson. 39*, 437–460.
Bhattacharyya, L., Freedman, J., Brewer, C. F., Brown, R. D., & Koenig, S. H. (1985) *Arch. Biochem. Biophys. 240*, 820–826.
Brudvig, G. W., Stevens, T. H., Morse, R. H., & Chan, S. I. (1981) *Biochemistry 20*, 3912–3921.
Buse, G., & Steffens, G. C. M. (1991) *J. Bioenerg. Biomembr. 23*, 269–289.
Calhoun, M. W. (1993) Ph.D. Thesis, University of Illinois, Urbana, IL.
Coffino, A. R., & Peisach, J. (1992) *J. Chem. Phys. 97*, 3072–3091.
Declercq, J.-P., Tinant, B., Parello, J., & Rambaud, J. (1991) *J. Mol. Biol. 220*, 1017–1039.
Drumheller, J. E., & Rubins, R. S. (1986) *J. Chem. Phys. 85*, 1699–1670.
Eads, C. D., LoBrutto, R., Kumar, A., & Villafranca, J. J. (1988) *Biochemistry 27*, 165–170.
Einarsdottir, O., & Caughey, W. S. (1985) *Biochem. Biophys. Res. Commun. 129*, 840–847.
Einspahr, H., Parks, E. H., Suguna, K., Subramanian, E., & Suddath, F. L. (1986) *J. Biol. Chem. 261*, 16518–16527.
Halkides, C. J., Farrer, C. T., Larsen, R. G., Redfield, A. G., & Singel, D. J. (1994) *Biochemistry 33*, 4019–4035.
Haltia, T. (1992) *Biochim. Biophys. Acta 1098*, 343–350.
Hansen, A. P., Britt, R. D., Klein, M. P., Bender, C. J., & Babcock, G. T. (1993) *Biochemistry 32*, 13718–13724.
Hardman, K. D., Agarwal, R. C., & Freiser, M. J. (1982) *J. Mol. Biol. 157*, 69–86.
Hartshore, D. J., & Boucher, L. J. (1974) in *Calcium Binding Proteins* (Drabikowski, W., Ed.) pp 30–49, Elsevier, Amsterdam.
Hosler, J. P., Fetter, J., Tecklenburg, M. M. J., Espe, M., Lerma, C., & Ferguson-Miller, S. (1992) *J. Biol. Chem. 267*, 24264–24272.
Hosler, J. P., Ferguson-Miller, S., Calhoun, M. W., Thomas, J. W., Hill, J., Lemieux, L., Ma, J., Georgiou, C., Fetter, J., Shapleigh, J. P., Tecklemburg, M. M. J., Babcock, G. T., & Gennis, R. B. (1993) *J. Bioenerg. Biomembr. 25*, 121–136.
Hosler, J. P., Shapleigh, J. P., Tecklenburg, M. M. J., Thomas, J. W., Kim, Y., Espe, M., Fetter, J., Babcock, G. T., Alben, J. O., Gennis, R. B., & Ferguson-Miller, S. (1994) *Biochemistry 33*, 1194–1201.
Hosler, J. P., Espe, M. P., Zhen, Y., Babcock, G. T., & Ferguson-Miller, S. (1995) *Biochemistry 34*, 7586–7592.
Jensen, P., Wilson, M. T., Aasa, R., & Malmstrom, B. G. (1984) *Biochem. J. 224*, 829–837.
Kelly, M., Lappalainen, P., Talbo, G., Haltia, T., van der Oost, J., & Saraste, M. (1993) *J. Biol. Chem. 268*, 16781–16787.
Kudynska, J., Zhang, Y. P., & Buckmaster, H. A. (1992) *J. Magn. Reson. 96*, 445–456.
Larsen, R. G., Halkides, C. J., Redfield, A. G., & Singel, D. J. (1992) *J. Am. Chem. Soc. 114*, 9608–9611.
Larsen, R. G., Halkides, C. J., & Singel, D. J. (1993) *J. Chem. Phys. 98*, 6704–6721.

Latwesen, D. G., Poe, M., Leigh, J. S., & Reed, G. H. (1992) *Biochemistry 31*, 4946−4950.
Lauraeus, M., Haltia, T., Saraste, M., & Wikstrom, M. (1991) *Eur. J. Biochem. 197*, 699−705.
Li, P. M., Gelles, J., Chan, S. I., Sullivan, R. J., & Scott, R. A. (1987) *Biochemistry 26*, 2091.
LoBrutto, R., Smithers, G. W., Reed, G. H., Orme-Johnson, B. H., Tan, S. L., & Leigh, J. S. (1986) *Biochemistry 25*, 5654−5660.
Ludwig, B. (1987) *FEMS Microbiol. Rev. 46*, 41−56.
Marcos, D., Folgado, J.-V., Beltran-Porter, D., Prado, M., Pulcinelli, S. H., & Almeida-Santos, R. H. (1990) *Polyhedron 9*, 2699−2704.
Markham, G. D., Nageswara, B. D., & Reed, G. H. (1979) *J. Magn. Reson. 33*, 595−602.
Martin, R. B. (1990) in *Metal Ions in Biological Systems 26* (Sigel, H., & Sigel, A., Eds.) pp 1−12, Marcel Dekker, New York.
McCracken, J., Peisach, J., Bhattacharyya, L., & Brewer, F. (1991) *Biochemistry 30*, 4486−4491.
McCracken, J., Shin, D. H., & Dye, J. L. (1992) *Appl. Magn. Reson. 3*, 305.
Meirovich, E., & Poupko, R. (1978) *J. Phys. Chem. 82*, 1920−1925.
Meirovitch, E., Brumberger, H., & Lis, H. (1978) *Biophys. Chem. 8*, 215−219.
Mims, W. B. (1984) *J. Magn. Reson. 59*, 291.
Mims, W. B., & Peisach, J. (1981) *Biol. Magn. Reson. 3*, 213−263.
Mims, W. B., Peisach, J., & Beinert, H. (1980) *J. Biol. Chem. 255*, 6843−6846.
Misra, S. K., & Sun, J.-S. (1991) *Magn. Reson. Rev. 16*, 57−100.
Mitchell, R., Brown, S., Mitchell, P., & Rich, P. R. (1992) *Biochim. Biophys. Acta* 1100, 40−48.
Moody, A. J., Cooper, C. E., & Rich, P. R. (1991) *Biochim. Biophys. Acta 1059*, 189−207.
Numata, M., Yamazaki, T., Fukumori, Y., & Yamanaka, T. (1989) *J. Biochem. 105*, 245−248.
Peisach, J., Mims, W. B., & Davis, J. L. (1979) *J. Biol. Chem. 254*, 12379−12389.
Reed, G. H., & Leyh, T. S. (1980) *Biochemistry 19*, 5472−5480.
Reed, G. H., & Markham, G. D. (1984) *Biol. Magn. Reson. 6*, 73−142.
Saraste, M. (1990) *Q. Rev. Biophys. 23*, 331−366.
Seelig, A., Ludwig, B., Seelig, J., & Schatz, G. (1981) *Biochim. Biophys. Acta 636*, 162−167.
Shaffer, J. S., Farach, H. A., & Poole, C. P., Jr. (1976) *Phys. Rev. B13*, 1869−1875.
Shapleigh, J. P., Hosler, J. P., Tecklenburg, M. M. J., Kim, Y., Babcock, G. T., Gennis, R. B., & Fersuson-Miller, S. (1992) *Proc. Natl. Acad. Sci. U.S.A. 89*, 4786−4790.
Smithers, G. W., Poe, M., Latwesen, D. G., & Reed, G. H. (1990) *Arch. Biochem. Biophys. 280*, 416−420.
Stevens, T. H., Martin, C. T., Wang, H., Brudvig, G. W., Scholes, C. P., & Chan, S. I. (1982) *J. Biol. Chem. 257*, 12106−12110.
Tipton, P. A., & Peisach, J. (1991) *Biochemistry 30*, 739−744.
Tipton, P. A., McCracken, J., Cornelius, J. B., & Peisach, J. (1989) *Biochemistry 28*, 5720−5728.
Weltner, W., Jr. (1983) *Magnetic Atoms and Molecules*, Van Nostrand Reinhold, New York.
Whitlow, M., Howard, A. J., Finzel, B. C., Poulos, T. L., Winborne, E., & Gilliland, G. L. (1991) *Proteins 9*, 153−173.
Yamashita, M. M., Almassy, R. J., Janson, C. A., Cascio, D., & Eisenberg, D. (1989) *J. Biol. Chem. 264*, 17681−17690.

BI9424757